Performance of a Focused Cavity Aerosol Spectrometer for Measurements in the Stratosphere of Particle Size in the 0.06–2.0-μm-Diameter Range

H. H. JONSSON,* J. C. WILSON,* C. A. BROCK,* R. G. KNOLLENBERG,† R. NEWTON,†
J. E. DYE,# D. BAUMGARDNER,# S. BORRMANN,@ G. V. FERRY,§ R. PUESCHEL,§
DAVE C. WOODS,** AND MIKE C. PITTS††

*Department of Engineering, University of Denver, Denver, Colorado
†Particle Measuring Systems, Inc., Boulder, Colorado
#National Center for Atmospheric Research, Boulder, Colorado
@University of Mainz, Mainz, Germany
§NASA Ames Research Center, Moffett Field, California
**NASA Langley Research Center, Hampton, Virginia
††Science Applications International Corporation, Hampton, Virginia

(Manuscript received 3 January 1994, in final form 21 June 1994)

ABSTRACT

A focused cavity aerosol spectrometer aboard a NASA ER-2 high-altitude aircraft provided high-resolution measurements of the size of the stratospheric particles in the 0.06–2.0-μm-diameter range in flights following the eruption of Mount Pinatubo in 1991. Effects of anisokinetic sampling and evaporation in the sampling system were accounted for by means adapted and specifically developed for this instrument. Calibrations with monodisperse aerosol particles provided the instrument's response matrix, which upon inversion during data reduction yielded the particle size distributions. The resultant dataset is internally consistent and generally shows agreement to within a factor of 2 with comparable measurements simultaneously obtained by a condensation nuclei counter, a forward-scattering spectrometer probe, and aerosol particle impactors, as well as with nearby extinction profiles obtained by satellite measurements and with lidar measurements of backscatter.

1. Introduction

A focused cavity aerosol spectrometer (FCAS), constructed by Particle Measuring Systems, Inc., in Boulder, Colorado, was operated for the first time on NASA's high-altitude research airplane, the ER-2, during the second Arctic Airborne Stratospheric Expedition (AASE II) in 1991–92. This expedition was undertaken partially to study the potential for ozone depletion in the stratosphere due to heterogeneous chemical reactions on the surfaces of aerosol particles. Accurate measurements of aerosol surface area concentrations were, therefore, essential. The FCAS, which is an improved version of an earlier ER-2 instrument, the passive cavity aerosol spectrometer (PCAS) (Wilson et al. 1992), measured the size distribution of the stratospheric sulfate particles resolved into 31 channels, with mean $\delta D/D$ of 0.111 (D being particle diameter). The main improvement over the PCAS involved focusing the laser beam inside the passive cavity to increase its intensity and extend the detection range of the instrument to smaller particle sizes. A forward-scattering spectrometer probe, FSSP-300, (Baumgardner et al. 1992), which sizes particles with diameters larger than 0.4 μm in diameter, and a condensation nuclei counter (CNC), which determines concentrations and mixing ratios of particles in the 0.01–1.0-μm-diameter range (Wilson et al. 1983), made simultaneous measurements on the ER-2. Additionally, an aerosol particle sampler (APS), a system of inertial wire impactors (Farlow et al. 1979; Pueschel et al. 1989), sampled particles on the ER-2 during the expedition.

The determination of aerosol particle size in the FCAS is based on the light-scattering properties of small spherical particles. The light scattered by a spherical particle that is not much larger than the wavelength of the incident light is a unique function of the particle's diameter and refractive index. A measurement of the light intensity scattered by a particle as it passes through a monochromatic beam of illumination of known intensity and wavelength thus reveals the particle's size provided its index of refraction is known. Since the composition of the stratospheric aerosol particles is predominantly sulfuric acid and water, the refractive index of the particles can be determined from temperature and water vapor measurements (Steele and

Corresponding author address: Dr. H. H. Jonsson, Dept. of Engineering, University of Denver, 2390 York Street, Denver, CO 80208.

Hamill 1981). Chan et al. (1989) describe the measurements of the local ambient state variables on the ER-2, and Kelly et al. (1989) describe the measurements of the water vapor mixing ratio.

In this paper we describe the FCAS and the methods used to reduce data from it. Also, we have undertaken comparisons with other relevant measurements to ascertain the validity of the data obtained with it. We considered this necessary because some of the corrections applied to the FCAS measurements could not be evaluated from first principles. Thus we are unable to provide quantitative estimates of our uncertainties without reference to external measurements. The comparisons indicate that the corrections applied to the data have produced a dataset that is consistent with other comparable particle measurements and is internally consistent throughout the expedition despite occasional changes to the instrument.

2. Instrument description

The optical bench of the FCAS is shown schematically in Fig. 1. Its main components are a high-order multimode He–Ne laser, a passive cavity, two sets of collecting (Mangin) mirrors, two linear photodiode detector arrays, an avalanche diode array for maximum sensitivity to size small particles, and a PIN (p-type silicon-intrinsic layer-n-type) diode array with sufficient sensitivity for detection of the larger particles. An output beam of about 5 mW intensity enters the passive cavity from the laser through an output coupler mirror and is focused to a waist of about 0.13 mm in diameter in front of the particle inlet. A small quartz crystal concave high-reflectivity mirror vibrating at 180 kHz causes the light to bounce back and forth in the cavity about 300 times driving up the intensity to 1–2 W and at the same time frequency shifting it to prevent interference with the laser source.

The particles enter the passive cavity through a 10-mm-long, 0.13-mm-wide slit orifice that is aligned with the laser. The Mangin mirrors, which are mounted opposite each other with circular apertures having collinear axes at right angles to the direction of the beam, collect the fraction of the light scattered by particles out of the laser beam into coaxial cones of 45° half-angles and project an image of the scatterer onto a section of the photodiode arrays. Each detector array consists of 12 linearly arranged photodiodes. As a small particle passes through a segment of the laser beam, its image is detected only by the particular array elements that view the beam segment the particle happens to be passing through.

The signals from the photodiode arrays are processed in three different ways. To maximize the signal-to-noise ratio for sizing of the smallest particles and at the same time maintain statistically significant counting rates at low particle concentrations, the electronics is designed to individually process signals from each avalanche diode element to isolate the one on which the particle is imaged. The background optical noise (Rayleigh scattering from air molecules) is thus decreased, as the

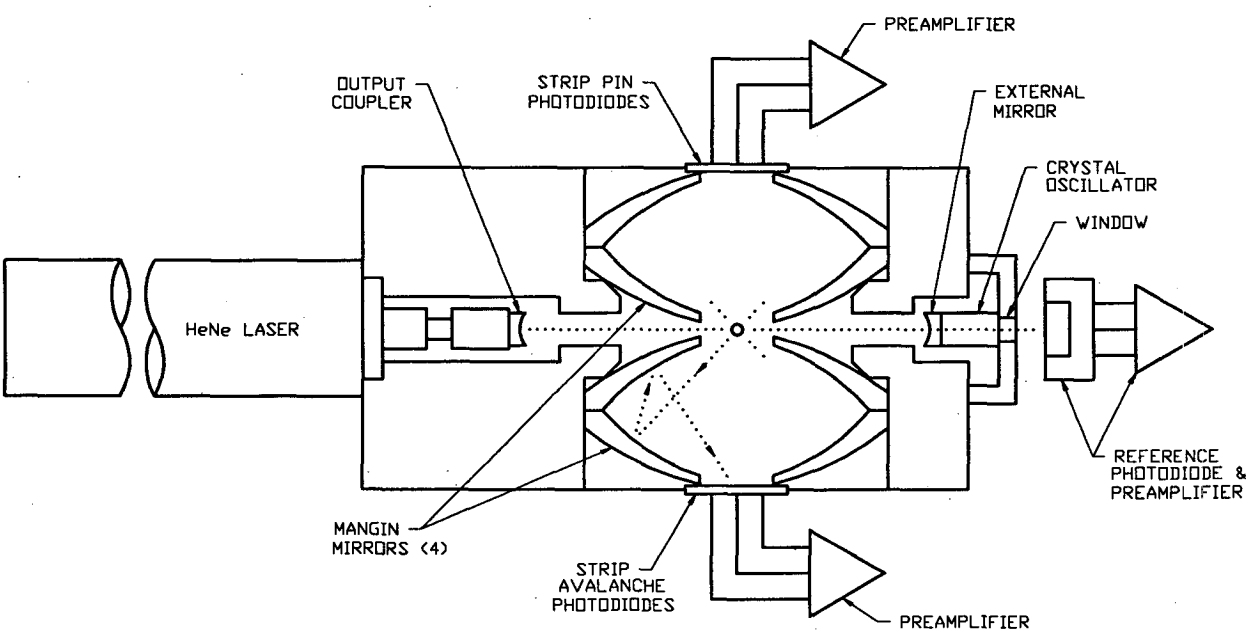

FIG. 1. The optical bench of the FCAS. The aerosol flow is out of the figure, through the segment of the laser beam between the apertures of the Mangin mirrors. An image of particles passing through this beam segment is cast onto the two photodiode arrays. In December 1991 a lens (not shown) was added in the laser path in front of the oscillating crystal mirror to minimize microphonics.

effective viewing volume thus shrinks to only one-twelfth (two-twelfths if the particle image falls onto two array elements) of the total beam length viewed. As a result, a sufficient signal to noise ratio is attained for detection and sizing of particles down to 0.06 μm in diameter. For particles this small, the scattered light intensity is proportional to the sixth power of the particle diameter. The signal amplifiers in this high gain section, therefore, quickly saturate as particle size increases. A second, lower gain, amplifier section becomes necessary for particles larger than about 0.1 μm in diameter. For particles this large, the signals from all 12 elements of the avalanche diode array are summed, and the signal sum is used to determine the particle size. This gain section saturates for particles larger than about 0.3 μm in diameter. For larger particles, the sum of the signals from the PIN diode elements is used to size the particles. The signals from the three different gain sections are passed to pulse height analyzers and logic circuitry where they are sorted into 31 size groups and counted over sampling periods of 10 s. Every 10 s a distribution of pulse heights is thus produced, which is translated into a particle size distribution during data reduction.

3. Sampling and transport

The aerosol sampling and flow system is shown schematically in Fig. 2. The aerosol is sampled through an inlet mounted on the skin of the airplane and aligned into the direction of the flow. The inlet contains two diffuser sections and has two corresponding sample extraction regions. This inlet system reduces the velocity of the sample from more than 200 m s^{-1} in the free airstream to less than 3 m s^{-1}. There are three processes associated with this speed reduction that may affect the particle measurements. First, the compression of the air associated with the speed reduction adiabatically heats the sample. Additional heating occurs as a result of conductive heat transfer from the optical cavity, which is maintained at 34°C. The heating thus produced can result in evaporation of volatile particle constituents. Depending on the particle composition, this may reduce the particle size or make particles volatilize altogether before they reach the cavity where their size is measured. Because of the low vapor pressure of sulfuric acid, most stratospheric particles survive this heating, but their diameter decreases and their acid mass fraction increases as water evaporates from them. Pure water or nitric acid trihydrate particles may be completely volatilized.

Another process associated with sampling that affects the measurements arises as inertia causes particles to cross the diverging flow streamlines in the sample extraction regions. Particles residing in air flowing past the diffusers may thus make their way into the aerosol sample and enhance the apparent particle concentration, particularly for large particles.

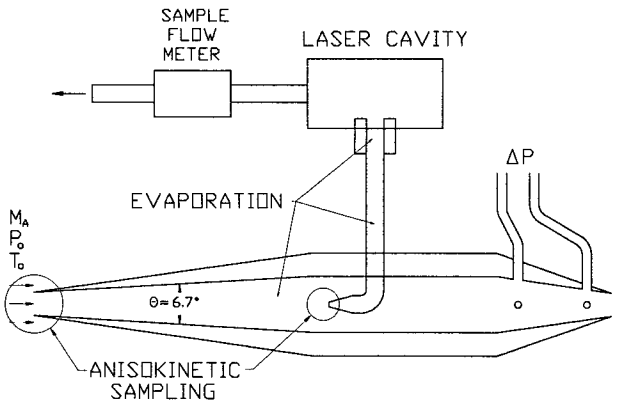

FIG. 2. The sampling system of the FCAS.

During the data reduction, we correct for errors that arise in measurements of particle size and in determination of particle concentration as a result of anisokinetic sampling and sample heating. To permit this correction, we measure the sample mass flow and the differential pressure in the convergent rear section of the main inlet from which the flow rate and temperature in the main section can be determined, knowing the ambient temperature and pressure and the airplane's speed.

Third, turbulent deposition on the wall of the diffuser can reduce the measured particle concentration (Huebert et al. 1990). Turbulence develops in diffusers having large area ratios (Brock et al. 1993a) and imparts momentum perpendicular to the inlet walls to particles in the airstream, increasing their chance of striking the walls and being removed from the sample. Current knowledge, however, does not permit prediction of turbulence or turbulent deposition in diffusers, but it is believed that the probability of turbulence is enhanced by misalignment of the inlet with the free stream flow. On one flight we checked this alignment by substituting a wind vector probe for the sampling inlet to measure the flow direction at its location during flight. The inlet alignment with the flow streamlines was found to be within 4°. The consistency (illustrated in a later section) of the FCAS measurements with results from the CNC, which uses a different inlet, and with results from the FSSP, which uses no inlet at all, suggests that particle losses on account of turbulence did not significantly reduce concentrations on the centerline of the main inlet where the sample is extracted.

4. Calibration and instrument response

The response of the FCAS depends on the refractive index of the aerosol particles. For determination of the instrument's response in stratospheric applications, we generated our calibration aerosol from a solution of di(2-ethylhexyl) sebacate and isopropyl alcohol using

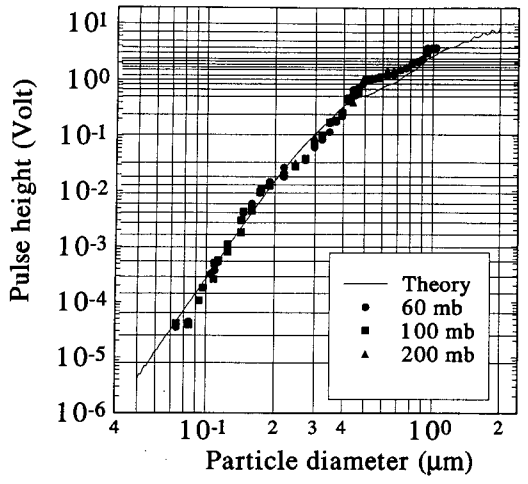

FIG. 3. Calibration of the FCAS. Horizontal lines represent channel boundaries.

a TSI collison atomizer (Liu and Lee 1975). The sebacate was used because it has a refractive index of 1.448, which is near that deduced from water vapor and temperature measurements for the stratospheric sulfate. The aerosol thus generated was diluted by filtered dry air, into which the alcohol evaporated, leaving a fairly broad size distribution of residual sebacate droplets. By use of a differential mobility analyzer (DMA) (Liu and Pui 1974), we extracted monomobile aerosol with a very narrow mobility distribution from the cloud of sebacate residuals. As aerosol particles exiting the DMA are mostly singly charged, the monomobile aerosol was usually also monodisperse although bimodal aerosol was occasionally used in the calibrations. The second mode appeared whenever a significant number of doubly charged particles passed through the DMA. The mean particle diameters in these modes could be controlled and selected to fall practically anywhere within the range of the FCAS up to diameter of about 1 μm.

To evaluate the performance of the FCAS in flight, we constructed a low-pressure chamber in which we could calibrate the instrument. At low ambient pressure, the ram pressure in the sampling inlet was found to contribute significantly to the pumping of the sample air through the instrument. At the same time the instrument's response appeared sensitive to the sample flow rate. It was, therefore, important in the calibrations to simulate not only the ambient pressure but also the in-flight ram pressure. During calibrations, the monodisperse aerosol was introduced directly to the slit inlet of the passive cavity without first passing through the sampling inlet. With this exception, the instrument was operated as if it were in flight.

Figure 3 shows a calibration of the FCAS and illustrates the instrument's dynamic range, which spans six orders of magnitude in optical signal. The vertical axis is the peak voltage of the signals resulting from the light scattered by particles passing through the laser beam. The mean diameter of the particles in the calibration aerosol is shown on the horizontal axis. The horizontal lines in the figure are not logarithmic grid lines but represent the voltage boundaries of the instrument's 31 channels. The line trace shows the theoretically expected response of the instrument based on Mie theory and the transfer function of the instrument's optics and electronics. The transfer function, however, was unknown and was determined by matching the calculated scattered intensities to the calibration. It is assumed to be independent of particle size. The dots represent geometric means of voltage pulses that formed the mode in the pulse distribution resulting from the calibration. The figure reveals some differences between the theoretically anticipated response of the instrument and the calibration points. Particularly, particles around 0.3 μm in diameter would be undersized and particles larger than 0.46 μm in diameter oversized if the theoretical response curve were used to determine particle sizes. The particle size boundaries used in the data reduction for individual channels, therefore, were defined by the intercepts of the voltage levels and a line drawn through the channel by channel calibration points shown and extrapolated to the highest channels with aid of the theoretical curve.

Figure 4 shows a typical response of the FCAS to a monodisperse aerosol sample. In this figure the horizontal axis has been converted from pulse heights to particle diameters in accordance with the calibration in Fig. 3. As the figure illustrates, many of the pulses, which in this case would be expected to have fallen into a mode around diameter of 0.58 μm, were systematically scattered into channels lower than anticipated. This occurred to some degree irrespective of the size of the calibration particles. We therefore determined

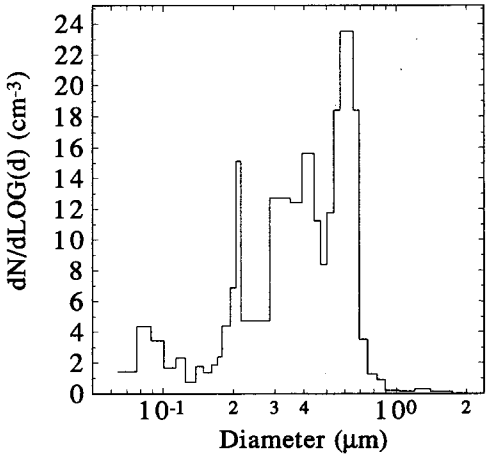

FIG. 4. The response of the FCAS to a monodisperse calibration aerosol with particles of mean diameter of 0.58 μm. Particles indicated as smaller than 0.50 μm are systematically undersized.

by calibrations with particles nominally sized for each channel the distribution of the resulting pulses. In this way we established the instrument's response matrices at various pressures. These matrices were used in the data reduction to retrieve undersized particles and place them in their proper size bins.

Table 1 shows the response matrix of the FCAS at 60-mb ambient pressure (i.e., near the ER-2's typical cruise level). The matrix is triangular because particles were only undersized. The diagonal values indicate the fraction of the particles correctly sized, and off-diagonal values are the fractions erroneously recorded in the lower channels. Particles detected in two channels adjacent to the targeted peak channel were considered to be correctly sized. This was necessary because the width of the calibration aerosol distribution was finite and usually larger than the width of the target channel. Thus it was difficult to determine for these channels what fraction of their counts was erroneous.

The response matrix of the FCAS was found to vary with pressure, ram pressure, and sample flow. In flight, however, both ram pressure and sample flow varied only with pressure in a highly reproducible manner such that a set of response matrices generated for given pressure levels using appropriate ram pressure and flow sufficed to convert the measured size distributions. A continuous pressure-dependent conversion was desired but practicality dictated that only a few response matrices could be used. Judged from a series of calibrations, three matrices were chosen to represent definite pressure intervals. The differences between the matrices, however, were small enough that no noticeable discontinuities appeared in the data stream at the arbitrary pressure boundaries as a consequence of the data-reduction routines switching from one matrix to another.

An ideal response matrix would be diagonal, indicating 100% sizing efficiency for every channel. In practice, however, such ideal response is rarely attained. There may be several reasons for the nonideal response of the FCAS. First, the laser beam is of similar width as the slit inlet, so if there is any widening of the aerosol jet after it enters the optical cavity, some of the particles may only pass through the edge of the beam and be partially illuminated. This would result in a reduced pulse height and an undersizing of the particles. Second, since the beam is multimodal, there are high-frequency local light intensity fluctuations within the beam itself. It is conceivable that particles may cross the beam at a time and location of such an intensity low and consequently be undersized. Finally, there are slight variations in the scattering geometry depending on the location of the scatterer within the viewing volume. The Mangin mirrors collect light scattered through slightly different angles from particles that enter the laser beam from the extremities of the slit inlet than from particles that enter it from the center, for instance. Since scattered light intensity is highly angle dependent, this may contribute to the variability in the instrument's response. Any or all of these may contribute to the nonideal response of the FCAS.

5. FCAS data reduction

a. Retrieval based on instrument's response

On the basis of the instrument's response matrices, the size distributions were retrieved using a simple iterative scheme. This was possible because of the triagonal nature of the response matrices and because the largest particles encountered in flight were almost invariably within the instrument's range. The highest channels invariably counted only a small fraction of the particles detected. If f_{ij} denotes the elements of the appropriate response matrix (the fractions of particles that should have fallen into channel i but fell into channel j), n_j the number of particles in channel j at the start of each iteration, and N_j the corrected number for channel j, then

$$N_i = \frac{n_i}{f_{ii}}$$

$$N_j = \frac{1}{f_{jj}}\left(n_j - \sum_{i=29}^{j+3} f_{ij}N_i\right): (i = 29, 28, 17, \cdots, 1;$$

$$j = i - 3, i - 4, \cdots, 1).$$

There were occasions when this resulted in a few negative counts in some channels, so a secondary iteration was done by checking for negative numbers. If any were found in a channel, then the count in that channel was brought back up to zero, while an equal number of counts was discarded from higher channels in the same proportion as these channels had received particles from the channel in question in the earlier iteration. Thus total particle count was conserved.

After correcting for the systematic particle undersizing, some apparently artificial irregularities frequently remained in the size distributions. The size distributions were, therefore, systematically smoothed by summing the particle counts in several groups of two or three adjacent channels and redistributing them such that equal $dN/d\log(d)$ values were assigned to each channel in a group.

b. Evaporation

The sampled aerosol particles were assumed to be liquid droplets composed of sulfuric acid and water. Numerous observations of particle composition have indicated that this assumption is valid at altitudes comparable with the ER-2's operating altitudes and reasonable down to the tropopause (see, e.g., Farlow et al. 1977; Gras and Laby 1978; Sheridan et al. 1992). It was furthermore assumed that the volatility of sul-

TABLE 1. The response matrix of the FCAS at 60 mb. Each column shows the fractional distribution of particles generated to fall into the channel corresponding to that column. For an ideally responding instrument, the matrix would be diagonal with each diagonal value equal to 1.0, but for the FCAS each column adds up to 1.0 as some fraction of the particles destined for the diagonal shows up in each of the lower channels.

	Channel number (i)																											
j	1	2	3	4	5	6	7	8	9	10	11	12	13	14	15	16	17	18	19	20	21	22	23	24	25	26	27	28	29
1	1			0.08	0.06	0.05	0.04	0.04	0.06	0.06	0.04	0.05	0.04	0.02	0.02	0.02	0.02	0.02	0.02	0.02	0.01	0.01	0.01	0.02	0.00	0.00	0.00	0.02	0.01
2		1			0.14	0.11	0.08	0.08	0.09	0.09	0.09	0.75	0.09	0.06	0.04	0.02	0.02	0.02	0.02	0.03	0.03	0.03	0.01	0.01	0.01	0.01	0.01	0.01	0.01
3			1			0.12	0.11	0.10	0.07	0.07	0.07	0.10	0.08	0.09	0.06	0.01	0.01	0.01	0.02	0.02	0.02	0.02	0.01	0.00	0.01	0.01	0.01	0.01	0.00
4				0.92			0.11	0.11	0.08	0.08	0.06	0.07	0.09	0.07	0.09	0.02	0.01	0.01	0.01	0.01	0.01	0.01	0.00	0.00	0.01	0.00	0.00	0.01	0.01
5					0.80			0.08	0.06	0.06	0.05	0.04	0.04	0.05	0.05	0.04	0.01	0.01	0.02	0.02	0.02	0.01	0.01	0.00	0.00	0.01	0.01	0.00	0.00
6						0.72			0.07	0.07	0.05	0.04	0.04	0.05	0.04	0.07	0.01	0.01	0.07	0.01	0.01	0.00	0.00	0.01	0.00	0.00	0.00	0.00	0.00
7							0.66			0.08	0.07	0.05	0.04	0.04	0.05	0.05	0.04	0.01	0.01	0.01	0.01	0.01	0.00	0.01	0.01	0.01	0.01	0.01	0.01
8								0.59			0.07	0.05	0.03	0.03	0.03	0.04	0.07	0.01	0.01	0.01	0.01	0.01	0.00	0.00	0.00	0.00	0.00	0.00	0.00
9									0.57			0.06	0.04	0.03	0.03	0.05	0.05	0.04	0.02	0.01	0.01	0.01	0.00	0.01	0.01	0.00	0.00	0.01	0.01
10										0.49			0.05	0.03	0.03	0.03	0.04	0.06	0.03	0.02	0.01	0.01	0.00	0.01	0.01	0.00	0.00	0.00	0.00
11											0.50			0.04	0.03	0.03	0.06	0.06	0.06	0.04	0.03	0.02	0.01	0.02	0.02	0.01	0.01	0.02	0.01
12												0.46			0.03	0.03	0.04	0.04	0.04	0.05	0.04	0.02	0.01	0.01	0.02	0.00	0.00	0.01	0.00
13													0.47			0.02	0.03	0.04	0.03	0.04	0.04	0.04	0.01	0.00	0.01	0.01	0.01	0.01	0.01
14														0.47			0.06	0.07	0.08	0.06	0.06	0.07	0.01	0.01	0.02	0.03	0.03	0.03	0.02
15															0.50			0.10	0.13	0.14	0.14	0.14	0.04	0.02	0.04	0.09	0.09	0.08	0.03
16																0.56			0.07	0.08	0.08	0.08	0.06	0.08	0.06	0.06	0.06	0.04	0.03
17																	0.52			0.09	0.09	0.10	0.10	0.15	0.15	0.10	0.10	0.05	0.06
18																		0.49			0.06	0.04	0.04	0.04	0.06	0.04	0.04	0.03	0.04
19																			0.43			0.03	0.03	0.03	0.03	0.03	0.03	0.03	0.03
20																				0.36			0.03	0.02	0.18	0.03	0.03	0.02	0.02
21																					0.33			0.03	0.03	0.02	0.02	0.03	0.03
22																						0.36			0.04	0.04	0.04	0.03	0.03
23																							0.63			0.02	0.02	0.01	0.01
24																								0.52			0.03	0.02	0.01
25																									0.46			0.02	0.01
26																										0.46			0.01
27																											0.44		
28																												0.50	
29																													0.60

furic acid is negligible. Then the ambient particle diameter d_{amb} is related to the measured diameter in the optical cavity d_{cav} by

$$d_{amb} = \left(\frac{f_{cav}\rho_{cav}}{f_{amb}\rho_{amb}}\right)^{1/3} d_{cav},$$

where f is the mass fraction of acid in the particle, and ρ is the particle's density.

If it is assumed that the particles are in equilibrium with the water vapor in their local environment, then, as shown by Steele and Hamill (1981) and Gmitro and Vermeulen (1963, 1964), the acid mass fraction of the particles f_{eq} and their density ρ_{eq} can be calculated from the temperature T and the water vapor pressure p_w. There can be little doubt that in the ambient environment the particles are in equilibrium with the water vapor; that is, $f_{amb} = f_{eq}(T_{amb}, p_{w,amb})$ and $\rho_{amb} = \rho_{eq}(T_{amb}, f_{amb})$. In the changing environment, however, during transport into the optical cavity, this assumption may not hold. To determine the composition of the particles after transport to the laser cavity, we ran a finite-difference model of the heat and mass exchange between the particles and their environment using the Fuchs and Sutugin (1970) transition regime flux interpolation. We ran the model for a range of stratospheric conditions and particle sizes. The results indicated that these processes occur with such rapidity that the particle acid mass fraction generally differed by less than 10% from the equilibrium acid mass fraction under cavity conditions at the time the particles cross the laser beam. On the basis of this result it appeared reasonable to assume that $f_{cav} = f_{eq}(T_{cav}, p_{w,cav})$ and $\rho_{cav} = \rho_{eq}(T_{cav}, f_{cav})$.

The Steele–Hamill and Gmitro–Vermeulen relations are based on measurements at relatively high temperatures and their utilization for stratospheric temperatures requires considerable extrapolations. Recent measurements of water vapor pressures over sulfuric acid solutions at stratospheric temperatures (Zhang et al. 1993), however, indicate that these extrapolations are reasonable.

c. *Sampling efficiency*

The sampling inlet and flow system of the FCAS are virtually the same as those that were used with an earlier ER-2 instrument, the passive cavity aerosol spectrometer, which was flown in AASE and was described by Wilson et al. (1992). The procedure developed then to correct for anisokinetic sampling was also used during AASE II. This correction involved calculation of the aspiration coefficients for the two diffusers of the sampling inlet from the flow measurements, using the empirical formula of Belyaev and Levin (1974) in combination with compressible flow theory to estimate flow rate in the main diffuser, thus reducing the sample concentrations accordingly.

During AASE II an opportunity arose to test the validity of this correction when a new pump was installed in the FCAS. The new pump increased the sample flow at low ambient pressure by almost a factor of 2, changing the anisokinetic correction at the inner diffuser by a similar amount. At this time the volcanic aerosol in the stratosphere had become well mixed throughout midlatitudes, and the particles had grown such that practically all of them were within the range of the FCAS. The CNC to FCAS number concentration ratio was thus fairly constant throughout northern midlatitudes and very close to unity.

In Table 2 we compare the total aspiration coefficient of the sampling system at cruising level on two 8-h flights; the 12 January 1992 flight (before the pump change) and the following 15 March flight (after the pump change). Also compared are the CNC/FCAS number concentration ratios obtained after the isokinetic correction had been applied to the FCAS data. The table shows that while the pump change resulted in more than 60% change in the total aspiration coefficient, or the magnitude of the anisokinetic correction, the indicated CNC/FCAS concentration ratios changed on average by only 11%. This small change in the concentration ratio is a strong indication that the anisokinetic correction is both appropriate and reasonably accurate.

d. *Optical and electronic noise*

Occasionally, noise appeared in some of the channels of the FCAS. This manifested itself in the appearance of clearly excessive particle counts in a particular channel in comparison with adjacent channels. In the early flights this was generally attributable to sensitivity of the optical system to vibrations transmitted from the airplane to the vibrating mirror in the passive cavity and interfering with its intentional vibration. This was remedied in December 1991.

At other times, noise was produced when a fiber or lint found its way into the cavity where it was caught in the narrow slit and flapped back and forth in the

TABLE 2. Comparison of CN to FCAS particle concentration ratios at ER-2 cruising altitudes on two flights when the anisokinetic correction for the FCAS measurements differed. The small change in the CN to FCAS concentration ratio associated with the much larger change in the anisokinetic correction attests to the appropriateness of the correction.

Flight date	FCAS average aspiration coefficient	Average CN:FCAS concentration ratio
1 December 1992	0.52 ± 0.031	1.22 ± 0.052
15 March 1992	0.84 ± 0.021	1.36 ± 0.065
Difference	62%	11%

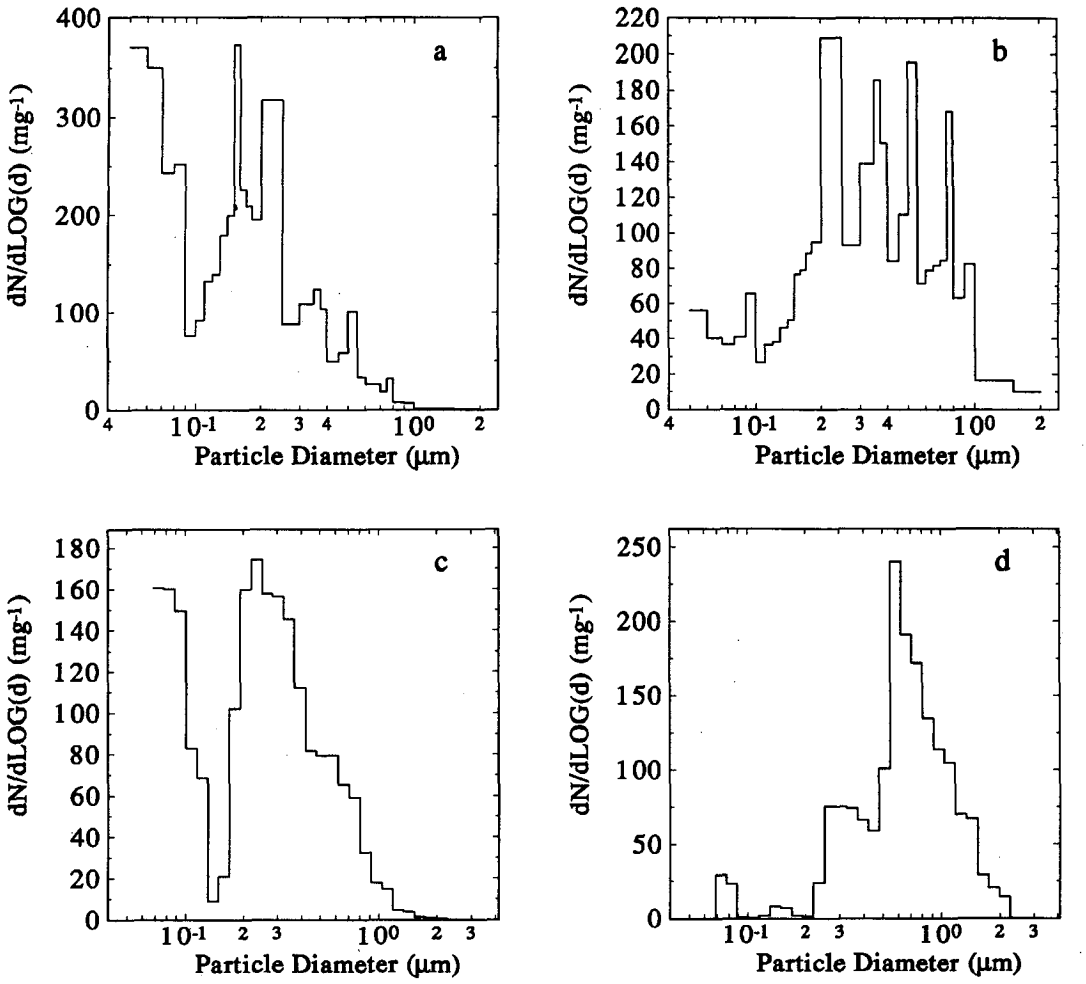

FIG. 5. Examples of the net effect of all the corrections applied to the FCAS measurements. The size distributions shown were obtained at 20-km altitude in October 1991 (the figures on the left-hand side) and in February 1992 (the figures on the right). The upper panels show uncorrected measurements and the lower panels show the same measurements after data reduction.

airstream, intercepting the laser beam and causing spurious optical signals. This instigated regular thorough cleansing of the slit inlet and the precaution that when the instrument was run in the laboratory or on the airplane on the ground only filtered air was admitted into the system. An additional source of noise appeared when the slit inlet was misaligned or inserted too far into the cavity such that a part of it became a source of scattered light. A careful alignment of the inlet with the laser beam was, therefore, very important. It was also noticed that during low-pressure calibrations, noise could sometimes be produced at will in selective channels by varying the pressure in the passive cavity. It appeared as though some components of the optical system were either flexing or shifting in their mounts, but inspection of the system failed to reveal the cause of this. There was hysteresis associated with this phenomenon such that if in-flight cavity pressure was approached from higher pressure values, some noise counts frequently remained present at flight conditions. If, on the other hand, the in-flight cavity pressure was approached from below, the noise was gone and the instrument zeroed in all channels at flight conditions upon sampling filtered air. Despite our general precautions to prevent an overpressurization of the cavity during calibrations prior to flights, noise, apparently of this nature, occurred in a few of the instrument's channels on the last two flights of the expedition.

Of 30 flights flown during AASE II, FCAS data for two entire flights were lost due to excessive electronic and optical noise. For four other flights in which noise occurred, corrections were applied. When spurious counts appeared in isolated channels, the entire particle count for the noisy channel was discarded. If the counts in surrounding channels appeared reliable, then a number was interpolated into the emptied channel,

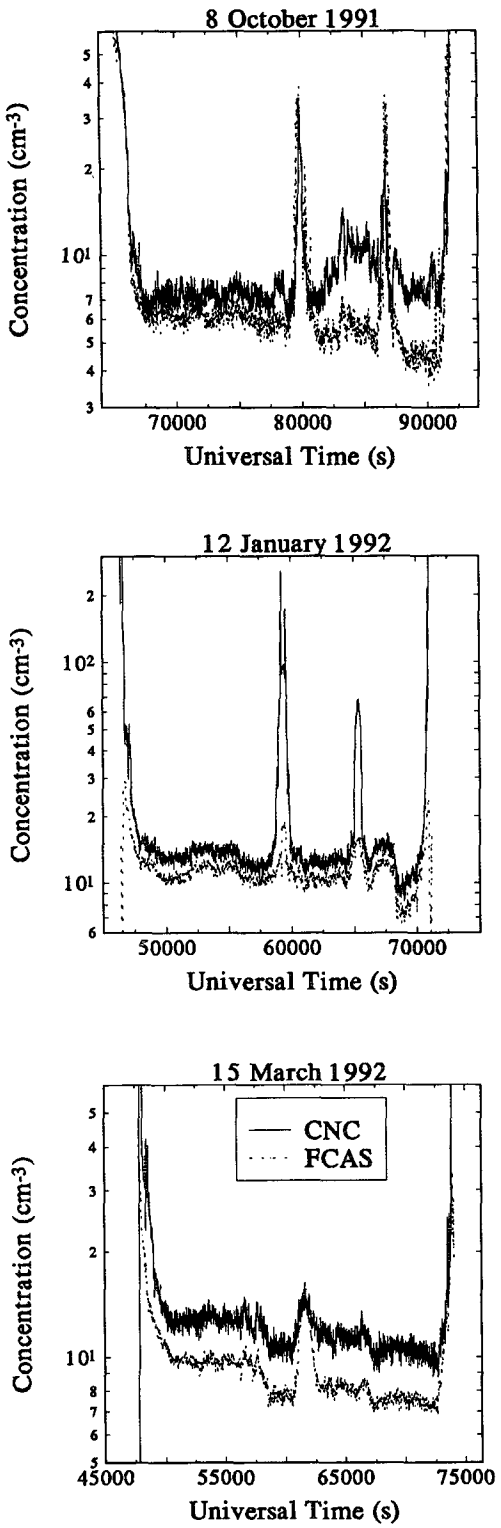

FIG. 6. Comparisons of FCAS number concentrations with CNC measurements on ER-2 flights. The excursions at the extremities of the curves occur during ascent and descent through the tropopause. Bumps, prominent in the October and January flights, occur as the airplane makes vertical excursions to sample a profile.

linearly in $dN/d\log(d)$. When noise appeared in channel 1, which counts the smallest detectable particles, or in channels 1 and 2, the count in these channels was simply discarded.

e. *Net effect of corrections*

Figure 5 illustrates the net effect of the data-reduction routines on the data. Figures 5a and 5b show raw size distributions obtained at 20-km altitude by the FCAS in October 1991 and February 1992, respectively. Figures 5c and 5d show the same size distributions after the data reduction. The corrected size distributions are smoother, the particle concentrations are lower on account of the anisokinetic sampling correction, and the particles are generally larger than in the raw data as a result of the evaporation correction and the nondiagonal instrument response. In the October flight, only 3.5 months after the eruption of Mount Pinatubo, the size distribution is bimodal, showing an accumulation mode with number mean diameter at about 0.2 μm and a nuclei mode that extends out of the detection range of the instrument. In the latter flight, eight months after the eruption, the aerosol has aged and become practically monomodal with number mean diameter of 0.8 μm. A more complete account of our observations of the impact of Mount Pinatubo on the stratospheric aerosol layer is to be found in Wilson et al. (1993) and Brock et al. (1993b).

6. Comparisons of FCAS data with other relevant measurements

a. *Comparison with the ER-2 CNC*

The detection range of the ER-2 CNC, 0.01–1 μm, overlaps broadly with the FCAS's range of 0.06–2.0 μm. Generally during the AASE II, the CNC indicated higher particle concentrations than the FCAS. Often, however, when the ER-2 sampled aged portions of Mount Pinatubo's plume where all the particles were expected to be in the size range detected by the FCAS, the particle concentrations indicated by the FCAS were within a few tens of percent of those indicated by the CNC. When the ER-2 flew into the Arctic polar vortex and when it climbed or descended into the tropopause region, the concentrations indicated by the two instruments usually diverged. At the same time, the FCAS typically showed a shift in the size distribution toward smaller sizes. In these cases some of the particles seen by the CNC fell below the detection range of the FCAS.

Figure 6 shows examples of particle concentrations obtained by the CNC and the FCAS. The figure illustrates the close agreement between the FCAS and the CNC throughout the expedition, with the FCAS most of the time showing slightly fewer particles than the CNC. Throughout the October flight (the top panel), the FCAS indicated bimodal size distributions with a

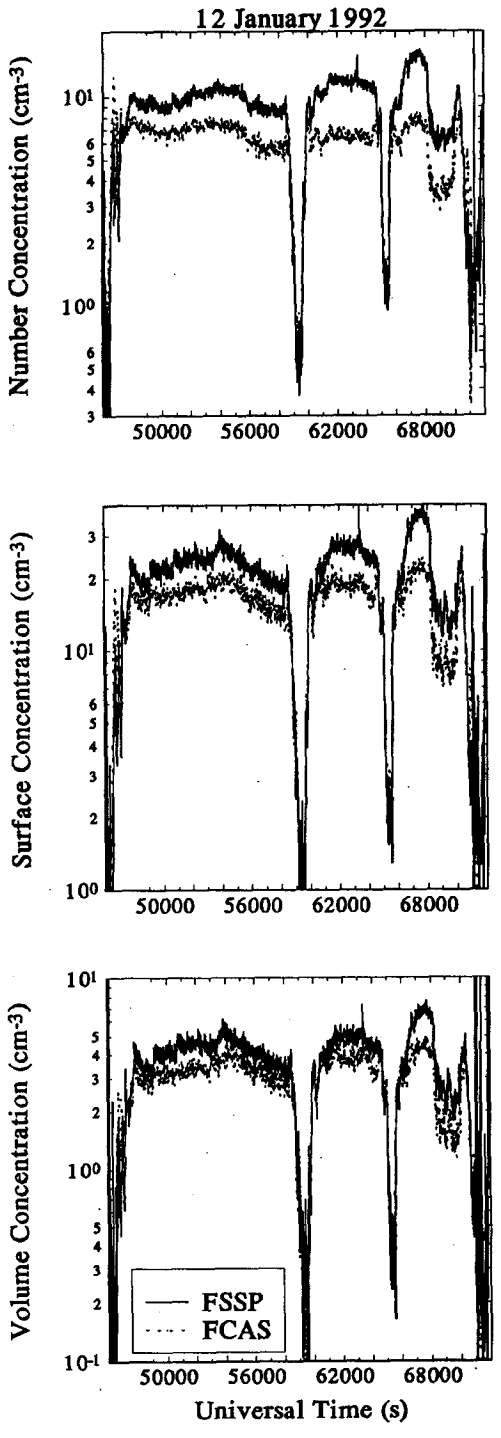

FIG. 7. Comparisons of FCAS number, surface, and volume concentrations with the corresponding quantities simultaneously obtained by the FSSP.

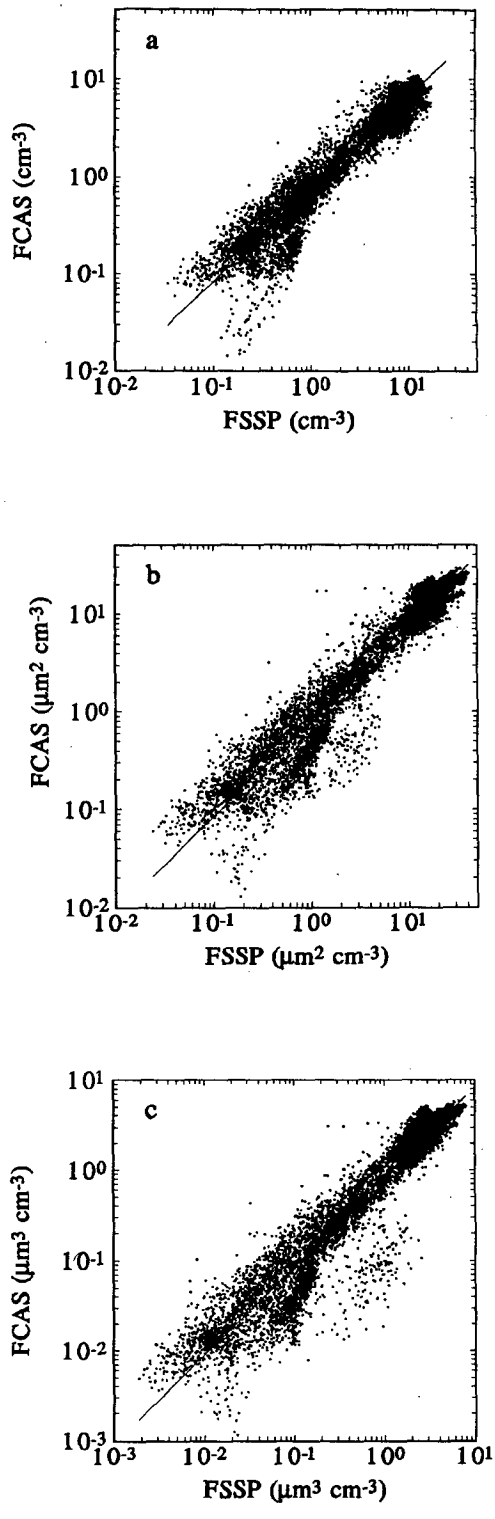

FIG. 8. Scatterplots of number, surface, and volume concentrations obtained by the FCAS against the corresponding quantities simultaneously obtained by the FSSP. The lines drawn through the data points were obtained by linear regression. They indicate FCAS/FSSP ratios of 0.62, 0.75, and 0.80 for the number, surface, and volume concentrations, respectively.

mode at or below the instrument's threshold. The divergence of the instruments in the second half of the flight might be attributed to an increased prominence

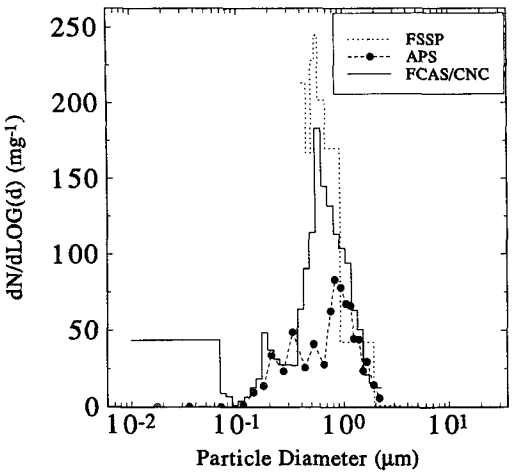

FIG. 9. Size distributions simultaneously obtained by the FCAS, FSSP, and APS at 20-km altitude in March 1992.

of this mode and a corresponding increase in the fraction of the particle concentration below the range of the FCAS. By January this entire mode had grown into the range of the FCAS and decreased relative to the larger particles' mode. The bumps in the CN curve in the January flight (center panel) occurred during the airplane's dips toward the tropopause. Associated with these dips was a shift in the particle size distribution toward smaller sizes below the range of the FCAS. Between the October and January flights, a lens had been installed inside the passive cavity of the FCAS to minimize noise on account of microphonics. In the March flight (bottom panel), in which the sample flow rate in the FCAS at cruising altitude was nearly a factor of 2 larger than in the earlier flights, the discrepancy between the two instruments is as before, generally in the 10%–20% range. From these graphs and others it may be concluded that despite two significant instrument changes during the mission, the FCAS measurements were consistent with the CNC measurements throughout the expedition.

b. Comparison with the ER-2 FSSP

The ER-2 FSSP-300 detects particles in the range from approximately 0.41–20.0-μm diameter and determines their sizes with a resolution of 31 channels. Sixteen FCAS channels overlap with the range of the FSSP.

Figure 7 shows an example of particle number (top panel), surface (center panel), and volume (bottom panel) concentrations calculated from FSSP data and the same quantities from the overlapping channels of the FCAS for a flight in January 1992. These graphs, which are typical for the entire expedition, indicate that generally slightly higher values were obtained by the FSSP than by the overlapping channels of the FCAS. Yet all the particles detected by the FSSP were within the range of the FCAS. The discrepancy is largest in the number concentrations, sometimes as large as a factor of 2, but is generally less than 30% for surface and volume concentrations. The figure shows this agreement holding as the concentrations vary through a range of two orders of magnitude.

Figure 8 shows scatterplots of the particle number (Fig. 8a), surface (Fig. 8b), and volume (Fig. 8c) concentrations obtained throughout the mission at ER-2 cruising altitudes by the overlapping channels of the FCAS against FSSP. Regression lines through the data points for the three aerosol parameters indicate systematic average discrepancies between the instruments. The FCAS reports on average 62% of the particles detected by the FSSP in the diameter range above 0.4 μm. The FCAS, however, reports 75% of the surface indicated by the FSSP and 80% of the aerosol volume, suggesting that the FCAS sizes the particles in this size range slightly larger on average than does the FSSP. These relationships between the instruments hold above pressure altitude of about 12 km, but below this level the surface area concentrations indicated by the two instruments diverge toward a factor of 2. This divergence is particularly marked in the early flights, but toward the end of the expedition this altitude sensitivity decreases. It is not clear what is causing this altitude dependence. The improvement in the later flights, however, coincides with and probably is largely attributable to the pump change in the FCAS in February 1992, after which the volume flow rate through the instrument became less sensitive to the ambient pressure. Another possible partial explanation, however, may also be sought in differences in the physical composition of particles near the tropopause and in the troposphere. Particles substantially volatile or containing substantial amounts of material other than sulfuric acid may not be accurately resized in the FCAS data reduction. Particles substantially different in composition from purely sulfuric acid and water may also have different refractive indexes from those assumed, which could result in sizing errors in either instrument. In the troposphere, the assumption that particles are sulfates, which is fundamental to the FCAS data reduction, can no longer be expected to hold, and discrepancies between the FCAS and FSSP are to be expected. At ER-2 cruising levels in the stratosphere, the differences between the instruments are small compared to the range of fluctuations in the aerosol properties observed during the mission.

The particle size distributions produced by the two instruments sometimes showed some inconsistencies in the details. Particularly, in the region of the lowest FSSP channels, more particles were counted by the FSSP than by the FCAS. In the early flights the discrepancy was particularly obvious when the airplane flew through the Pinatubo cloud, but toward the end

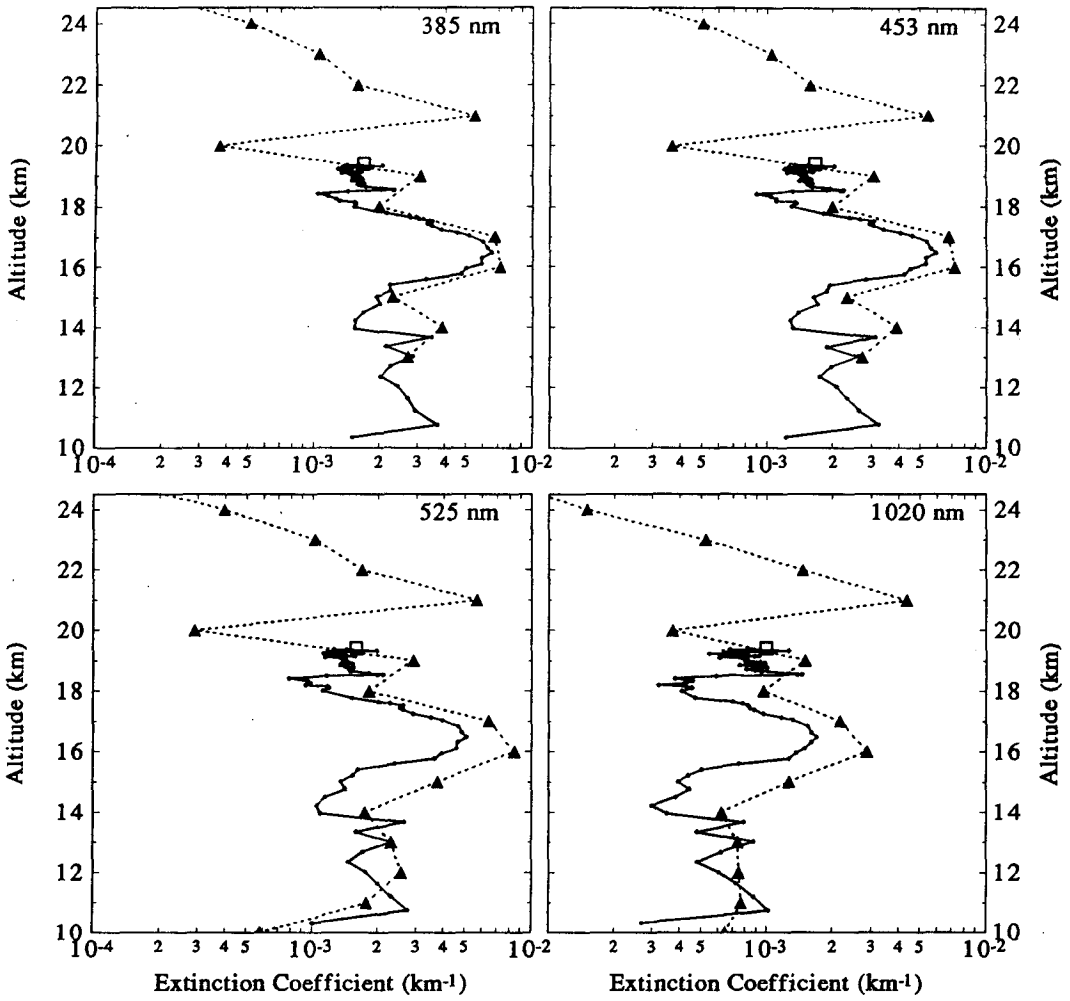

FIG. 10. Extinction profiles calculated from FCAS particle size distributions using the four SAGE II wavelengths compared with SAGE II measurements. The relevant SAGE wavelengths are indicated in the upper right corner of each panel. The FCAS profile was obtained upon ascent from Moffett Field, California, (solid line) on 4 October 1991. The SAGE II profile was obtained 2.5 h earlier, 500 km farther north (filled triangles, dotted line). An open square represents ER-2 measurement obtained in level flight as it crossed the latitude of the SAGE II profile 240 km east of it.

of the mission the agreement in the details of the overlapping region improved. Throughout the mission, nevertheless, the two instruments closely agreed on the location of the mode of the size distribution whenever it was located within the overlapping region of the instruments' ranges.

c. *Comparison with the ER-2 APS*

The Ames aerosol particle samplers were regularly flown on the ER-2 during the AASE II. The impactor wires are exposed to the free airstream where they inertially collect particles from the air. The wires are then brought to the laboratory where the residues of the collected particles are analyzed under an electron microscope for determination of particle size and composition. The collection efficiency of the wires depends on airplane speed and altitude and on wire diameter, particle mass, and particle phase. The collection efficiency for liquid particles is known from both theory and experiment and is used in the reduction of the data, but solid particles may bounce off the wires upon impact and are therefore expected to be less efficiently collected. The analyses of the wires yield particle number concentrations and size distributions, as well as information on particle composition.

Figure 9 shows size distributions obtained simultaneously by the FCAS, FSSP, and APS at 20-km altitude on the 15 March 1992. The number of CN in excess of that measured by the FCAS is indicated as a single

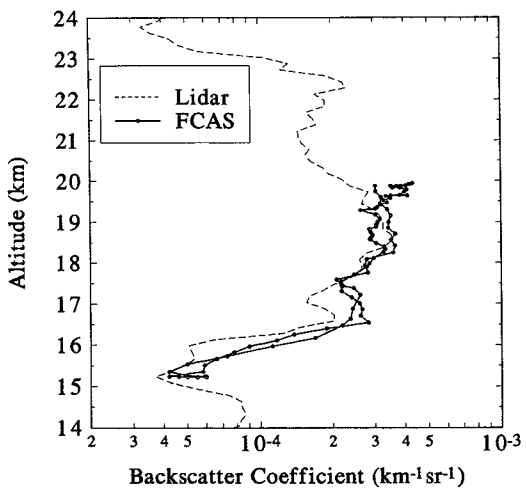

FIG. 11. Comparison of a profile of the backscatter coefficient measured by 694-nm lidar at NASA's Langley Research Center with a calculated profile for the lidar wavelength using coordinated FCAS measured particle size distributions.

channel count in the 0.01–0.07-μm range. As the figure illustrates, the FSSP indicates more particles in the range between 0.4 and 0.9 μm than either the FCAS or the APS. The APS shows a significant particle deficit compared to the optical spectrometers in this range. The FCAS, on the other hand, shows slightly more particles larger than 0.9 μm than either of the other systems. Below 0.4 μm, the APS and the FCAS appear in good agreement, but the small nuclei mode indicated by the excess CNC counts is absent in the APS size distribution. This comparison is typical for the approximately 20 APS size distributions available for comparison. Overall, there is an agreement between the FCAS and the APS in the location of particle modes in cases when the nuclei mode is absent, but particle concentrations obtained by the two techniques sometimes differ by as much as a factor of 2.

d. Comparison with satellite measurements of extinction

On several occasions during the expedition, the ER-2 sampled regions of the atmosphere in close spatial and temporal proximity with an extinction profile from the Stratospheric Aerosol and Gas Experiment II (SAGE II) aboard the earth radiation budget satellite. Using the aerosol size distributions measured by the FCAS, the extinction coefficient was calculated in these instances for the four wavelengths used by the satellite. Figure 10 shows extinction profiles thus obtained. The ER-2 profile is obtained during ascent from Moffett Field (36.6°N, 123°W at 62 279 s UTs) on the 4 October 1991, while the SAGE II profile is taken 2.5 h earlier and farther north (43.4°N, 131°E at 53 309 UTs). At this time the effect of Mount Pinatubo's eruption still manifested itself in plumes and laminae throughout the stratosphere, so strong horizontal gradients in extinction were frequently encountered. Nevertheless, both systems reveal similar stratification in the stratospheric aerosol, although sometimes there is up to a factor of 2 disagreement in the values obtained.

Other occasions when the ER-2, while in level flight, flew near a SAGE extinction profile measurement are shown in Table 3. For these cases the ER-2 pressure altitude was hypsometrically converted to geopotential height to correspond with the satellite altitudes. Corresponding SAGE extinction values were obtained for the ER-2 altitude by linear interpolation between the two neighboring measurements reported above and below the flight altitude. The extinctions generally agree to within 40%, often within 10%. An exception is the 14 October 1991 case, in which discrepancy of nearly a factor of 2 is observed. Examination of the horizontal distribution of extinction along the ER-2 trajectory on this day revealed an order of magnitude variation in extinction in the region explored by the satellite. In the half-hour following the measurement reported in Table 3, the extinction calculated from the FCAS mea-

TABLE 3. Comparison of extinction obtained from particle size distributions measured by the FCAS to extinctions obtained by the SAGE II. A negative time difference indicates that the ER-2 measurement was done before the SAGE II measurement. A negative difference between the two measurements indicates ER-2 extinction values lower than those obtained by SAGE II.

			Wavelengths			
Flight date	Time difference (s)	Distance (km)	385 nm (% diff)	453 nm (% diff)	525 nm (% diff)	1020 nm (% diff)
4 October 1991	−11 920	404	28.2	28.7	28.1	27.7
14 October 1991	−14 118	295	67.5	67.4	68.1	68.9
20 January 1992	26 049	88	8.0	11.5	17.1	8.5
	5036	74	39.7	39.5	41.2	39.1
15 March 1992	−28 496	126	13.6	17.2	17.6	4.1
18 March 1992	−12 734	372	−36.6	−11.4	−1.5	−24.0
	−33 114	372	4.1	4.2	6.2	−12.7
	−6785	1700	−61.2	−15.4	−1.6	−13.7
	−27 535	1700	12.1	11.8	11.9	−9.4

surements increased from the 67%–68% of the SAGE measurement to nearly twice the SAGE value. In this particular case the inhomogeneity of the aerosol makes the comparison difficult.

e. Comparison with lidar

During the ER-2 flight on 12 January 1991, a profile was coordinated with the operation of a 694-nm lidar at NASA's Langley Research Center in Virginia. The lidar obtained a backscatter profile near daybreak, and in the afternoon the ER-2 made a dip that was planned by aid of forecast isentropic air trajectories to occur in the same air parcel the lidar examined earlier in the day. Figure 11 shows the profile of the backscatter coefficient measured by the lidar and a backscatter profile calculated for the lidar wavelength from the aerosol size distributions measured by the FCAS. The two independent measurements reveal almost identical structure and an agreement well within a factor of 2 in values throughout the overlapping altitudes.

7. Summary and conclusions

A novel focused cavity aerosol spectrometer was operated aboard NASA's ER-2 high-altitude aircraft during the second Arctic Airborne Stratospheric Expedition during the fall of 1991 and the winter of 1992. The instrument provided high-resolution size distributions of the sulfate particles in the stratosphere following the volcanic eruption of Mount Pinatubo. The instrument detected and sized sulfate particles in the range from 0.06 to 2.0 μm in diameter at altitudes of up to 20 km.

Intercomparisons show consistency in the FCAS measurements with measurements obtained by a variety of other techniques. Systematic differences between the FCAS and the FSSP may be due to errors in either system. The less than 40% systematic difference in particle number, 25% difference in particle surface, and 20% difference in particle volume represent an improvement from an earlier ER-2 expedition where an unresolved discrepancy of a factor of 2 occurred between the FSSP and a passive cavity aerosol spectrometer. The comparisons with the SAGE II extinction measurements and the Langley lidar reveal that the FCAS measurements are providing a similar description of the optical properties of the stratospheric aerosol, not only qualitatively but quantitatively, to within a factor of 2.

It may be concluded from the intercomparisons that as a result of our effort in accounting for sampling artifacts the FCAS measurements provided a consistent, coherent, dataset on the properties of the stratospheric aerosol in the fall of 1991 and the winter of 1992. The importance of this is exemplified by the fact that in June 1991 Mount Pinatubo in the Philippines emitted an estimated 20 megatons of sulfur dioxide into the stratosphere. The FCAS flew successfully on 26 ER-2 flights from August 1991 to March 1993 and covered the latitudes from 23°N to the North Pole. The dataset it produced thus presents an excellent opportunity to study the evolution and implications of this extraordinary geological event.

Acknowledgments. We thank Lamar Kirchhevel for helping us with the artwork. We also thank Dave Gesler and Rick Heiden for their work on the wind vector measurement. This work was supported by NASA Upper Atmosphere Research Program Grant NAG-2-458.

REFERENCES

Baumgardner, D., J. E. Dye, B. W. Gandrud, and R. G. Knollenberg, 1992: Interpretation of measurements made by the forward scattering spectrometer probe (FSSP-300) during the airborne arctic stratospheric expedition. *J. Geophys. Res.*, **97,** 8035–8046.

Belyaev, S. P., and L. M. Levin, 1974: Techniques for collection of representative aerosol samples. *J. Atmos. Sci.*, **5,** 325–338.

Brock, C. A., J. C. Wilson, and W. R. Seebaugh, 1993a: *Aerosol Measurement: Principles, Techniques, and Applications.* Van Nostrand Reinhold, 690–704.

——, H. H. Jonsson, J. C. Wilson, J. E. Dye, D. Baumgardner, S. Borrmann, M. C. Pitts, M. Osborn, R. J. DeCoursey, and D. C. Woods, 1993b: Relationships between optical extinction, backscatter and aerosol surface and volume in the stratosphere following the eruption of Mt. Pinatubo. *Geophys. Res. Lett.*, **20,** 2555–2558.

Chan, K. R., S. G. Scott, T. P. Bui, S. W. Bowen, and J. Day, 1989: Temperature and horizontal wind measurements on the ER-2 aircraft during the Airborne Antarctic Ozone Experiment. *J. Geophys. Res.*, **94,** 11 573–11 587.

Farlow, N. J. D., M. Hayes, and H. Y. Lem, 1977: Stratospheric aerosols: Undissolved granules and physical state. *J. Geophys. Res.*, **82,** 4921–4929.

Farlow, N. H., G. V. Ferry, H. Y. Lem, and D. M. Hayes, 1979: Latitudinal variations of stratospheric aerosols. *J. Geophys. Res.*, **84,** 733–743.

Fuchs, N. A., and A. G. Sutugin, 1970: *Highly Dispersed Aerosols.* Ann Arbor Science, 105 pp.

Gmitro, J. I., and T. Vermeulen, 1963: Vapor-liquid equilibria for aqueous sulfuric acid. University of California, Lawrence Radiation Laboratory, Report URCL-10886, 181 pp.

——, and ——, 1964: Vapor–liquid equilibria for aqueous sulfuric acid. *AIChE J.*, **10,** 740–746.

Gras, J. L., and J. E. Laby, 1978: Southern Hemisphere stratospheric aerosol measurements. 1: Simultaneous impactor and in situ single-particle (light scatter) detection. *J. Geophys. Res.*, **83,** 1869–1874.

Huebert, B. J., G. Lee, and W. L. Warren, 1990: Airborne aerosol inlet efficiency measurement. *J. Geophys. Res.*, **95,** 16 369–16 381.

Kelly, K. K., and Coauthors, 1989: Dehydration in the lower Antarctic stratosphere during late winter and early spring. 1987. *J. Geophys. Res.*, **94,** 11 317–11 357.

Liu, B. Y. H., and D. Y. H. Pui, 1974: A submicron aerosol standard and the primary, absolute calibration of the condensation nuclei counter. *J. Colloid. Interface Sci.*, **47,** 155–171.

——, and K. W. Lee, 1975: An aerosol generator of high stability. *Amer. Ind. Hyg. Assoc. J.*, **36,** 861–865.

Pueschel, R. F., and Coauthors, 1989: Condensed nitrate, sulfate, and chloride in Antarctic stratospheric aerosols. *J. Geophys. Res.*, **94,** 11 271–11 284.

Sheridan, P. J., R. C. Schnell, D. J. Hofmann, and T. Deshler, 1992: Electron microscope studies of Mt. Pinatubo aerosol layers over Laramie, Wyoming, during summer 1991. *Geophys. Res. Lett.*, **19,** 203–206.

Steele, H. M., and P. Hamill, 1981: Effects of temperature and humidity on the growth and optical properties of sulfuric acid-water droplets in the stratosphere. *J. Aerosol Sci.*, **12,** 517–528.

Wilson, J. C., J. H. Hyun, and E. D. Blackshear, 1983: The function and response of an improved stratospheric condensation nucleus counter. *J. Geophys. Res.*, **88,** 6781–6785.

——, M. R. Stolzenburg, W. E. Clark, M. Loewenstein, G. V. Ferry, K. R. Chan, and K. K. Kelly, 1992: Stratospheric sulfate aerosol in and near the Northern Hemisphere polar vortex: The morphology of the sulfate layer, multimodal size distributions, and the effect of denitrification. *J. Geophys. Res.*, **97,** 7997–8013.

——, and Coauthors, 1993: In situ observations of the stratospheric aerosol following the eruption of Mt. Pinatubo. *Science,* **261,** 1140–1143.

Zhang, R., P. J. Wooldridge, J. P. D. Abbatt, and M. J. Molina, 1993: Physical chemistry of H_2SO_4/H_2O binary system at low temperatures: Stratospheric implications. *J. Phys. Chem.*, **97,** 7351–7358.